

AERODYNAMIC MECHANISMS ON A GROUND-MOUNTED SOLAR PANEL AT DIFFERENT WIND DIRECTIONS

Onur YEMENİCİ * 

Received: 18.02.2020; revised: 27.02.2020; accepted: 05.03.2020

Abstract: Aerodynamics mechanisms on a solar panel were studied using Computational Fluid Dynamics methodology at different wind directions. The wind velocity was chosen as 10 m/s that corresponding turbulent flow. The inclination angle of the panel was fixed as 25°, while the wind directions were varied as 180°, 135°, 45°, and 0°. Governing equations were solved by utilizing a finite volume method with a realizable k-ε turbulence model and standard wall functions. The results showed that the recirculation area occurred for the straight wind directions, but it was not observed for the oblique wind directions. The highest pressure coefficients occurred at the leading edges of the solar panel and they reduced to the trailing edge for all wind directions. The maximum drag and uplift coefficient was obtained at the wind direction of 0° and 180°, respectively.

Keywords: Wind Direction, Computational Fluids Dynamics, Wind Loads, Solar Panel

Farklı Rüzgar Yönlerinde Yere Monte Bir Güneş Panelinde Aerodinamik Mekanizmalar

Oz: Bir güneş panelindeki aerodinamik mekanizmalar, farklı rüzgar yönlerinde Hesaplamalı Akışkanlar Dinamiği kullanılarak incelenmiştir. Rüzgar hızı, türbülanslı akışa karşılık gelen 10m/ s olarak seçilmiştir. Panelin eğim açısı 25° olarak sabitlenirken, rüzgar yönleri 180°, 135°, 45° ve 0° olarak değiştirilmiştir. Korunum denklemleri, realizable k-ε türbülans modeli ve standart duvar fonksiyonları ile sonlu hacim yöntemi kullanılarak çözülmüştür. Sonuçlar, yeniden dolaşım bölgesinin düz rüzgar yönlerinde meydana geldiğini, ancak eğik rüzgar yönleri için gözlemlenmediğini göstermiştir. En yüksek basınç katsayıları panelin ön kenarlarında meydana gelmiş ve daha sonra tüm rüzgar yönleri için arka kenara doğru azalmıştır. 0° ve 180° rüzgar yönleri, maksimum sürüklenme ve kaldırma açısından sırasıyla kritik bulunmuştur.

Anahtar Kelimeler: Rüzgar Yönü, Hesaplamalı Akışkanlar Dinamiği, Rüzgar Yüğü, Güneş Paneli

1. INTRODUCTION

Since energy demands are growing day by day, alternative energy research increases along with that. Solar energy is a reliable source, but it is a challenge to make cost-efficient and effective solar panels in comparison to traditional energy resources. Therefore, there have been many investigations on optimization studies of solar panels recently, such as Aly and Bitsuamlak (2013) carried out wind tunnel study for geometric scale effect on solar panels mounted on a low-rise building. They showed that the size of the model was not changed with the mean pressure loads. Kopp et al. (2012) examined the solar panel arrays that mounted on the roof and ground with the different inclination angles of the panel in a wind tunnel. They found that turbulence generated by the panels and pressure equalization were two main mechanisms causing the aerodynamic loads. Bitsuamlak et al. (2010) performed a study to investigate the

* Uludağ University, Engineering Faculty, Department of Mechanical Engineering, 16059, Bursa, Turkey
Correspondence Author: Onur YEMENİCİ (oseckin@uludag.edu.tr)

wind angle effects on ground-mounted solar panels. The numerical results showed that the pressure coefficients were similar patterns, while the magnitudes of the pressure coefficients were underestimated to compare to full-scale measurements. Jubayer and Hangan (2016) performed simulations to determine the wind loads for different wind directions on the solar panels. They reported that the highest values of the C_D and C_L were determined on the first row for all four wind directions, while the maximum overturning moments occurred for the 45° and 135° wind directions. Shademan et al. (2014) performed CFD simulations to investigate the unsteady wind loads of the panels with the effects of ground clearance. They found that the bigger clearance caused higher wind loads and shedding frequencies, and stronger vortex shedding. CFD analyses were performed to analyze the wind loads of solar panel arrays at different wind angles of attack and panel inclination angles by Shaderman and Hangan (2010), who found that the simulations identified the corner panels as the critical ones, and the entire structure experienced the largest wind loading for azimuthal wind directions of 0° and 180° . Jubayer and Hangan (2012) examined wind loads of the ground-mounted panels in an atmospheric boundary layer numerically. They reported that flow separation was not occurred on the top of the panel, while the support structure caused two vortices on the lower surface of the panel. Stenabaugh et al. (2015) studied the wind loads of the panel arrays which mounted on the roof of the buildings. Pratt and Kopp (2013) performed velocity measurements on the solar panel arrays that mounted to roof for various wind angles of attack and investigated the flow field around the panels. Agarwal et al. (2017) performed a numerical study on the coefficients of the drag and lift of a panel for various wind angles, and reported that the highest negative and maximum positive C_p values found for the wind angle of 60° and 90° , and 0° and 45° on the windward and the leeward side, respectively.

A numerical investigation was performed for wind loads on a solar panel at the various wind directions of 180° , 135° , 45° , and 0° , in this study.

2. METHOD AND APPROACH

In this section, numerical modeling setup, the panel geometry, boundary conditions, and computational domain dimensions were explained. The dimension of the panel with a 25° inclination angle was in length of 1 m, in width of 0.7 m, and in thickness of 0.025 m. The back support height of the panel was 1.3 m, and the height of the front supports was dimensioned according to the angle of panel inclination. The panel geometry and computational domain were modeled using the SOLID-WORKS design software package. The dimensions of the computational domain were $21H$ in length, $11H$ in width, and $5H$ in height, and the distance of the inlet area to supports was $7H$, as given in Figure 1.

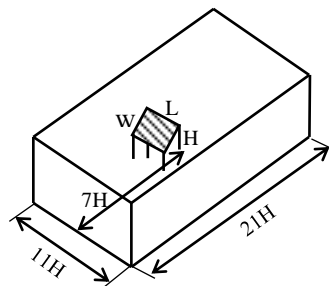


Figure 1:
The solar panel in the computational domain

The incompressible and unsteady continuity and momentum equations can be written as follows:

$$\frac{\partial u_i}{\partial x_i} = 0 \quad (1)$$

$$\rho \frac{\partial u_i u_j}{\partial x_j} = -\frac{\partial P}{\partial x_i} + \mu \frac{\partial}{\partial x_j} \left(\frac{\partial u_i}{\partial x_j} + \frac{\partial u_j}{\partial x_i} \right) + \rho \frac{\partial}{\partial x_j} (-\overline{u'_i u'_j}) \quad (2)$$

The term of Reynolds stress $-\overline{u'_i u'_j}$ is described by the following equations:

$$-\overline{u'_i u'_j} = \mu_t \left(\frac{\partial u_i}{\partial x_j} + \frac{\partial u_j}{\partial x_i} \right) \quad (3)$$

where μ_t represents turbulent viscosity. The simulations were carried out with the realizable k- ϵ model. k is turbulence kinetic energy, and ϵ is dissipation rate. The three-dimensional realizable k- ϵ model is widely applied in CFD, especially to analyze complex flows with large strain rates such as recirculation, rotation, and separation. Eq. (4) and (5) defined the transport equations as,

$$\frac{\partial}{\partial t} (\rho k) + \rho \frac{\partial}{\partial x_i} (k u_i) = \frac{\partial}{\partial x_i} \left[\left(\mu + \frac{\mu_t}{\sigma_k} \right) \frac{\partial k}{\partial x_j} \right] + P_k + P_b - \rho \epsilon - Y_M + S_k \quad (4)$$

where,

$$\frac{\partial}{\partial t} (\rho \epsilon) + \rho \frac{\partial}{\partial x_i} (\epsilon u_i) = \frac{\partial}{\partial x_j} \left[\left(\mu + \frac{\mu_t}{\sigma_\epsilon} \right) \frac{\partial \epsilon}{\partial x_j} \right] + \rho C_1 S_\epsilon - \rho C_2 \frac{\epsilon^2}{k + \sqrt{\nu \epsilon}} + C_{1\epsilon} \frac{\epsilon^2}{k} C_{3\epsilon} P_b + S_\epsilon \quad (5)$$

$$C_1 = \max \left[0.43, \frac{\eta}{\eta + 5} \right], \eta = S \frac{k}{\epsilon}, S = \sqrt{2 S_{ij} S_{ij}} \text{ and } S_{ij} = \frac{1}{2} \left(\frac{\partial u_j}{\partial x_i} + \frac{\partial u_i}{\partial x_j} \right)$$

P_k and P_b is the turbulence kinetic energy generation because of the velocity gradients and buoyancy, respectively, which are both estimated as the standard k- ϵ model. The rate of the turbulence fluctuating to the entire dissipation rate is defined as Y_M . The values of $C_{1\epsilon}$, $C_{2\epsilon}$, σ_k , and σ_ϵ are 1.44, 1.9, 1.0, and 1.2, respectively. A standard wall function is employed with near-wall treatment.

The mesh was consisting of 1.3 million cells generated with ANSYS meshing, as shown in Figure 2. In the inlet domain, 10 m/s wind speed of and 5% turbulence intensity was chosen. The bottom surface of the domain, support structures, and panel was modeled as a no-slip rough wall, while the sides and top of the domain were considered as no-slip smooth walls. Zero gradients of pressure were applied at the outlet of the domain.

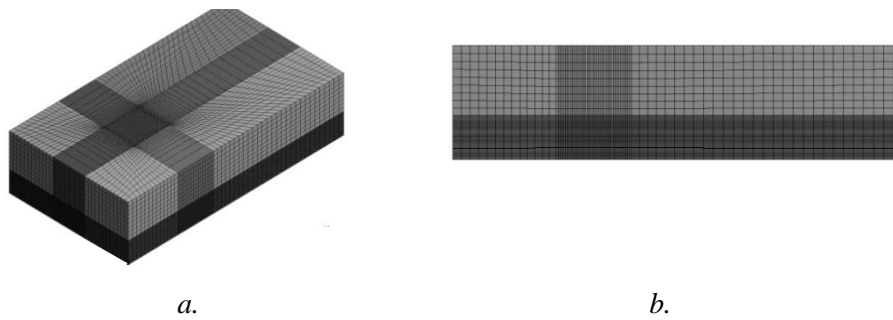
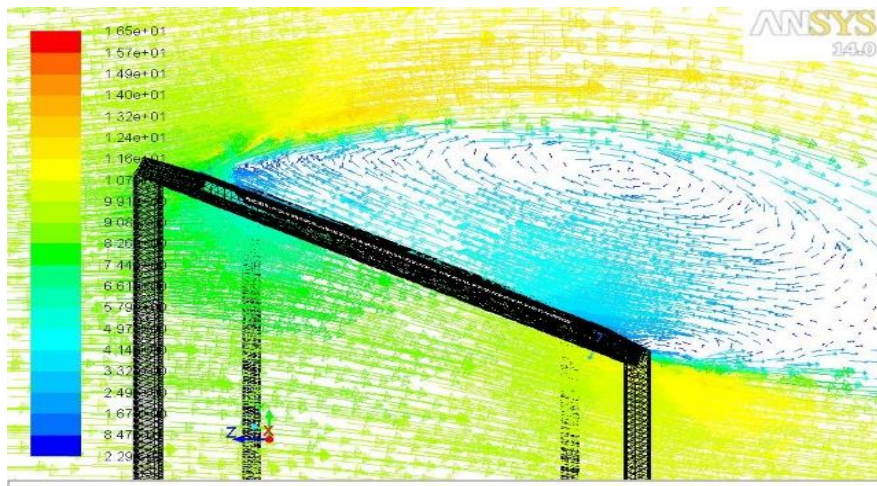


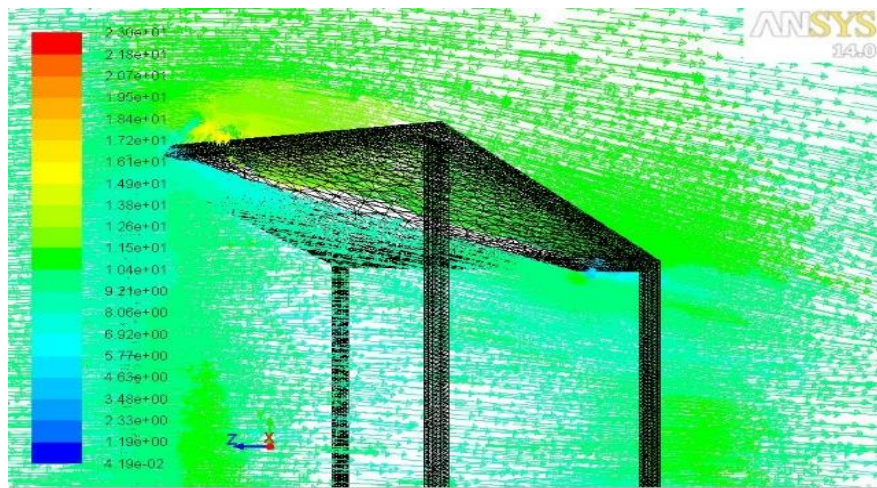
Figure 2:
The mesh of the computational domain;
a. *Isometric view* **b.** *Side view*

3. RESULTS AND DISCUSSION

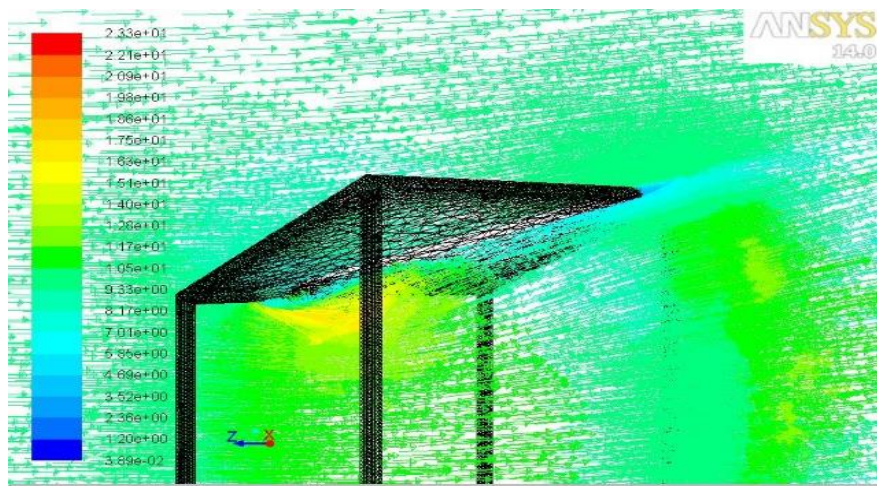
The simulations were conducted on a ground-mounted panel for 10 m/s wind speed at 25° panel inclination angle and four various wind directions. The flow fields of the panel were shown in Figure 3 a-d for the wind directions of 180°, 135°, 45°, and 0°, respectively. The leading edges of the panel for all wind directions were exposed to the relatively low speed of the wind as it's the stagnation point of the panel. The velocity around the leading edge was between 5-6 m/s and 8-9 m/s in straight (180° and 0°) and oblique (135° and 45°) wind directions, respectively. A recirculation area occurred at the straight wind directions, but it was not observed for the 135° and 45° wind directions. The recirculation area was obtained on the lower surface of the panel for the wind direction of 0°, while it occurred at the top surface of the panel for the wind direction of 180°. Only one vortex was observed for the straight wind directions. The flow accelerated as it moved through the trailing edge of the panel for straight wind directions. However, the effect of acceleration was observed on lower and upper surface for 180° and 0° wind direction, respectively. Even though velocity distributions were well proportioned in oblique wind directions, maximum velocities could be seen right after leading edges. For 45° wind direction, it occurred beneath the lower surface of the panel, while it was above the top surface of the panel for the wind direction of 135°. So, the flow behavior for straight and oblique wind directions was similar due to the symmetric distribution.



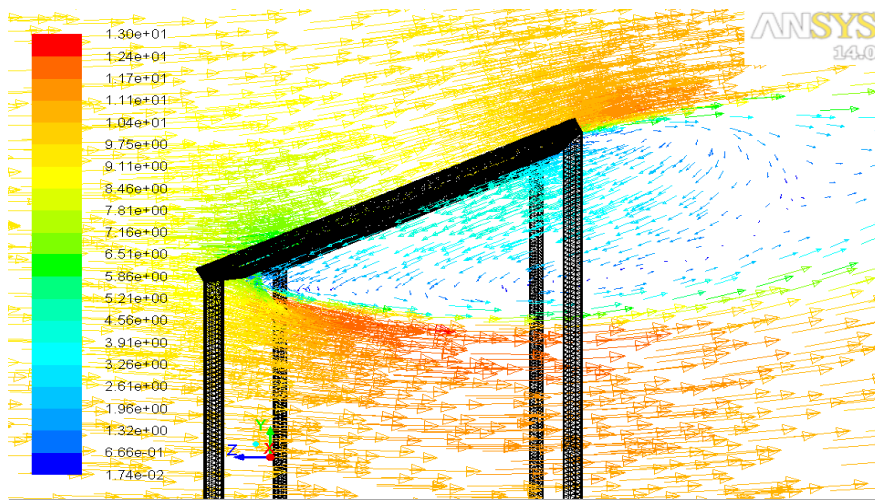
a.



b.



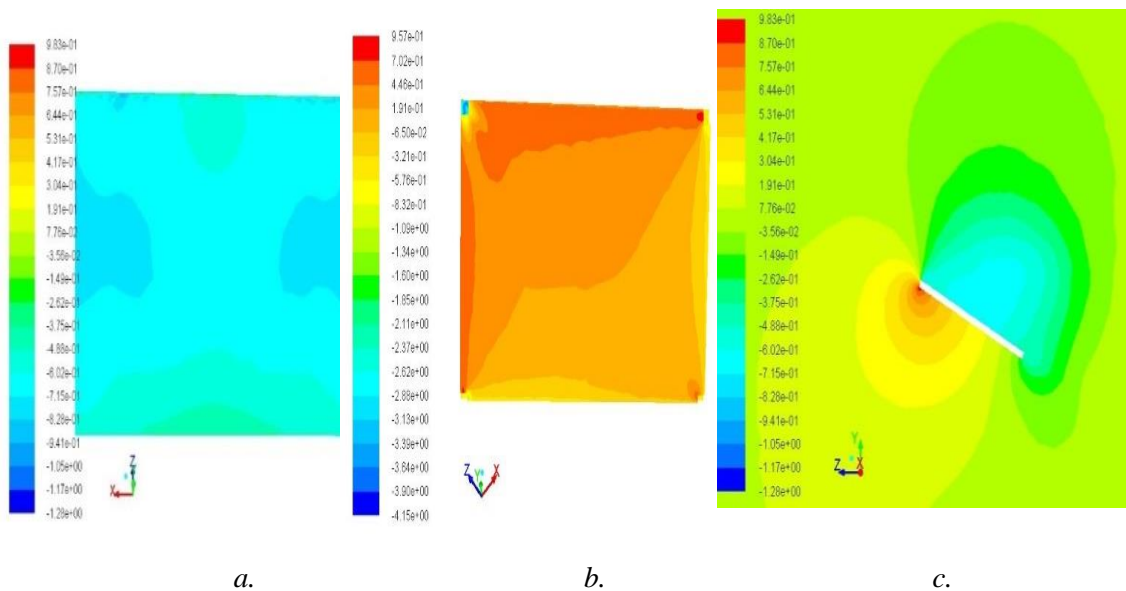
c.



d.

Figure 3:
Velocity vectors around the panel
a. 180°, b. 135°, c. 45° and d. 0° wind directions

The pressure coefficient distributions on the panel for the wind directions of 180° and 0° are given in Figures 4 and 5, respectively. It was observed that as flow accelerated, Cp values were tending to decrease at both wind directions. The highest pressure coefficient occurred as 0.98 at the leading edge of the upper surface for the wind direction of 0°, where the flow separation occurred. The Cp values decreased monotonically from the leading to trailing edge. The lower surfaces exposed to the wind at 180° wind direction, as opposed to 0° wind directions. For the wind direction of 180°, the highest pressure coefficient determined as 0.94 at the leading edge of the lower surface. The maximum Cp in absolute values for straight winds was found very close, as expected.



a. b. c.
Figure 4:
Pressure coefficient values for 180° wind direction on
a. upper surface, b. lower surface, and c. sides of the panel

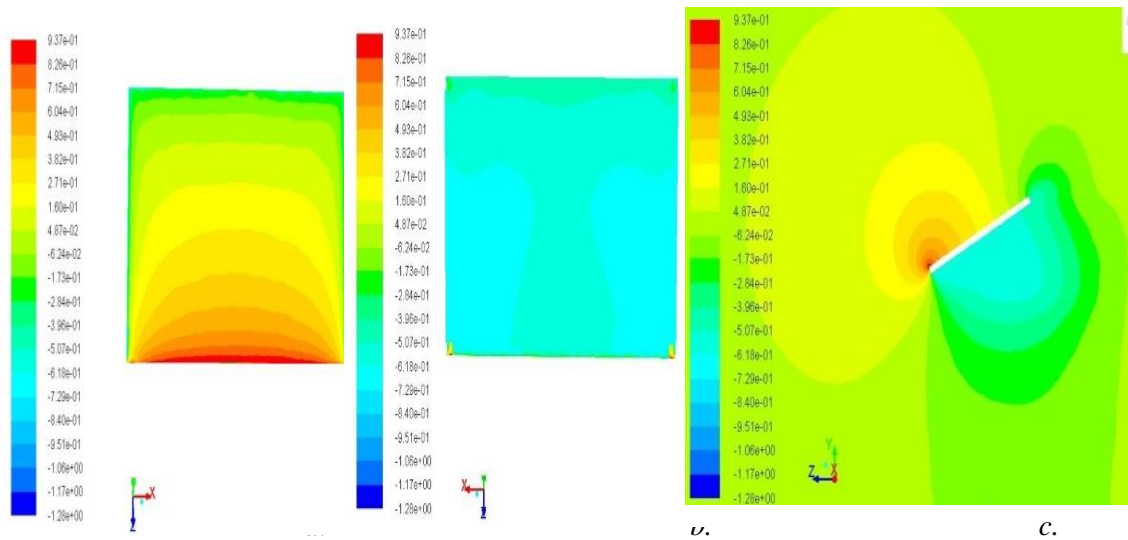


Figure 5:
*Pressure coefficient values for 0° wind direction on
a. upper surface, b. lower surface, and c. sides of the panel*

Figure 6 and 7 shows the pressure coefficients for the wind directions of 45° and 135°, respectively. The wind directions of 45°-135° were chosen to analyze non-uniform wind exposure. The Cp values decreased as flow accelerated at both wind directions, and asymmetrical Cp distributions were observed for oblique winds. The highest Cp values were generated at the leading edge of the upper and lower surface for 45° and 135° wind directions, respectively. The maximum Cp in absolute values of the panel was 0.68 and 0.70 for the wind directions of 45° and 135°, respectively.

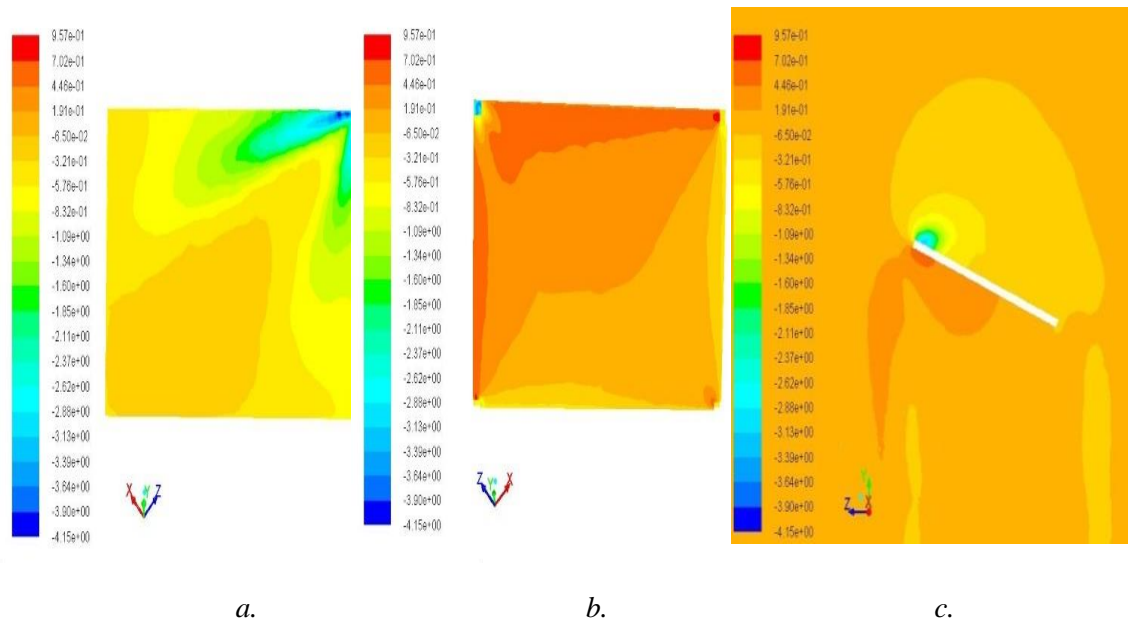


Figure 6:
*Pressure coefficient values for 135° wind direction on
a. upper surface, b. lower surface, and c. sides of the panel*

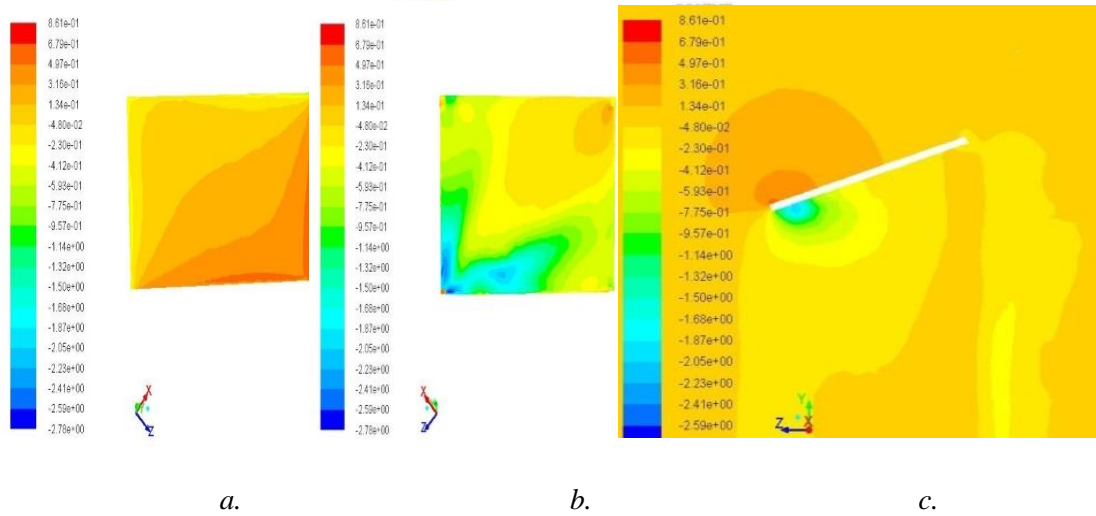


Figure 7:
 Pressure coefficient values for 45° wind direction on
 a. upper surface, b. lower surface, and c. sides of the panel

Figure 8 shows the mean values of lift and drag coefficients by wind directions. The mean values of C_D of the panel were calculated as 0.482, 0.397, 0.428, and 0.563 for the wind directions of 180°, 135°, 45°, and 0°. The maximum drag coefficient was obtained for the wind direction of 0° as the wind flows to the panel normally. The C_D values were higher for straight winds than oblique winds. The smallest drag coefficient was determined for the wind direction of 135°. The mean lift coefficients determined as 0.708, 0.584, -0.629 and -0.828 for the wind directions of 180°, 135°, 45°, and 0°, respectively. The negative C_L values were obtained for the wind directions of 45° and 0°, while the positive lift values were determined for the wind directions of 135° and 180°. The maximum negative and positive lift was found for 0° and 180° wind directions, respectively. The C_L values of the panel for straight wind directions were higher than those of values of oblique wind directions, as in the drag coefficients.

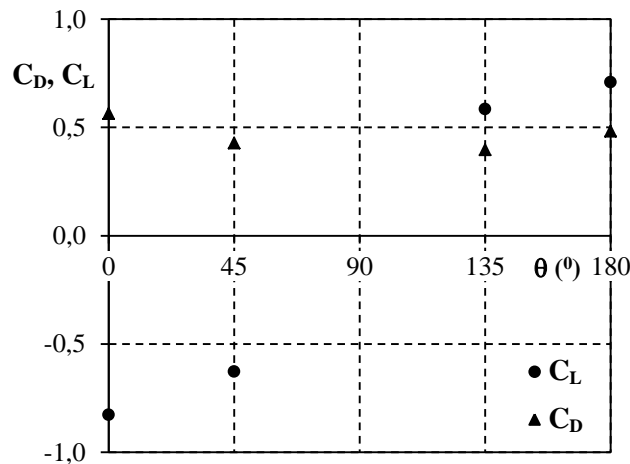


Figure 8:
 The lift and drag coefficients

4. CONCLUSIONS

This study was carried out to specify the effects of the wind direction on a solar panel numerically. The wind velocity and panel inclination angle were chosen as 10 m/s and 25° respectively, while the wind directions were varied as 180°, 135°, 45°, and 0°.

It was found that the recirculation areas occurred only at the straight wind directions, which were seen on the top and bottom panel surface for the 180° and 0° wind directions, respectively. The maximum velocities were found to be where the minimum pressure coefficients occurred for all wind directions.

For all wind directions, the highest pressure coefficients obtained at the leading edge of the solar panel, and the values dropped monotonically to the trailing edge. The symmetric C_p distributions were obtained for the wind directions of 180° and 0°, while the distributions were asymmetrical for 135° and 45° wind directions.

The highest drag coefficient was obtained for 0° wind direction, while the smallest value found for 135° wind direction. The negative C_L values were occurred for 45° and 0° wind directions, while the positive lift values were determined for the wind directions of 135° and 180°. The maximum negative and positive lift was obtained for 0° and 180° wind directions, respectively. The values of the pressure, lift, and drag coefficients were higher for straight wind directions than oblique wind directions.

REFERENCES

1. Agarwal, A., Irtaza, H. and Zameel, A. (2017) Numerical study of lift and drag coefficients on a ground-mounted photo-voltaic solar panel. *Materials Today: Proceedings*, 4, 9822-9827. doi:10.1016/j.matpr.2017.06.274
2. Aly, A.M. and Bitsuamlak, G. (2013) Aerodynamic loads on solar panels, *Western University, Structures Congress*, 1555-1564. doi: 10.1061/9780784412848.137
3. Bitsuamlak, G.T., Dagneu, A.K. and Erwin, J. (2010) Evaluation of wind loads on solar panel modules using CFD, *The Fifth International Symposium on Computational Wind Engineering*, USA, May 23-27.
4. Jubayer, C.M. and Hangan, H. (2012) Numerical Simulation of Wind Loading on Photovoltaic Panels, *University of Western Ontario, Structures Congress*, 1180-1188. doi: 10.1061/9780784412367.106
5. Jubayer, C.M. and Hangan, H. (2016) A numerical approach to the investigation of wind loading on an array of ground mounted solar photovoltaic (PV) panels, *Journal of Wind Engineering and Industrial Aerodynamics*, 153, 60-70. doi: 10.1016/j.jweia.2016.03.009
6. Kopp, G.A., Farquhar, S. and Morrison, M.J. (2012) Aerodynamic mechanisms for wind loads on tilted, roof-mounted, solar arrays, *Journal of Wind Engineering and Industrial Aerodynamics*, 111, 40-52. doi: 10.1016/j.jweia.2012.08.004
7. Pratt, R.N. and Kopp G.A. (2013) Velocity measurements around low-profile, tilted, solar arrays mounted on large flat-roofs, for wall normal wind directions, *Journal of Wind Engineering and Industrial Aerodynamics*, 123, 226-238. doi: 10.1016/j.jweia.2013.09.001
8. Shademan, M. and Hangan, H. (2010) Wind loading on solar panels at different azimuthal and inclination angles. *The Fifth International Symposium on Computational Wind Engineering*, USA, May 23-27.
9. Shademan, M., Balachandar, R. and Barron, R.M. (2014) Detached eddy simulation of flow past an isolated inclined solar panel, *Journal of Fluids and Structures*, 50, 217-230. doi: 10.1016/j.jfluidstructs.2014.06.024

10. Stenabaugh, S.E., Iida, Y., Kopp, G.A. and Karava, P. (2015) Wind loads on photovoltaic arrays mounted parallel to sloped roofs on low-rise buildings. *Journal of Wind Engineering and Industrial Aerodynamics*, 139, 16-26. doi: 10.1016/j.jweia.2015.01.007